

## SPECIAL ISSUE ARTICLE

# Short fiber spraying process of all-oxide ceramic matrix composites: A parameter study

Jonas Winkelbauer  | Georg Puchas | Walter Krenkel | Stefan Schafföner 

Ceramic Materials Engineering (CME),  
University of Bayreuth, Bayreuth,  
Germany

## Correspondence

Jonas Winkelbauer, Ceramic Materials  
Engineering, University of Bayreuth,  
Prof.-Rüdiger-Bormann-Str. 1, 95447  
Bayreuth, Germany.

Email:

[Jonas.Winkelbauer@uni-bayreuth.de](mailto:Jonas.Winkelbauer@uni-bayreuth.de)

## Abstract

Fiber spraying processes have been established for polymer matrix composites for decades. In this study, we transferred an automated fiber spraying process to short fiber bundle-reinforced Nextel 610/  $\text{Al}_2\text{O}_3$ - $\text{ZrO}_2$  oxide fiber composites (SF-OFC). The effect of the processing factors travel height, spray angle, and movement speed on the specimen strength was analyzed in a full factorial experimental design. As a result, the significance of the travel height as well as the interaction between travel height and movement speed was demonstrated. Furthermore, the influence of the fiber length (14, 28, 56, and 112 mm) on the bending stress and strain was investigated. Independent of the used fiber length, the SF-OFC exhibited an excellent quasi-ductile fracture behavior with bending strains in the range of .6% and in-plane isotropic material properties. The average bending strength increased from  $133 \pm 27$  MPa with 14 mm fiber reinforcements to  $163 \pm 29$  MPa with 112 mm fibers. The achieved bending strengths clearly exceeded the off-axis properties of currently used fabric-reinforced OFC. These properties, combined with the excellent drapability and cost effectiveness, make the novel material highly promising for industrial applications such as flame tubes, burner nozzles, kiln furnitures, or foundry components.

## KEYWORDS

ceramic matrix composites, composites, fabrication, fibers, oxides, spraying process

## 1 | INTRODUCTION

Oxide fiber composites (OFC) combine lightweight construction potential with excellent thermomechanical properties in oxidizing and corrosive atmospheres at temperatures up to  $1100^\circ\text{C}$ .<sup>1</sup> Due to their general availability and simple processing, OFCs are mostly manufactured by using fabric reinforcements.<sup>2–16</sup> These two-dimensional textile preforms are made of high-performance oxide fibers such as Nextel 610 and Nextel 720 and enable

quasi-ductile fracture behavior of the OFCs compared to brittle fracturing monolithic ceramics. The quasi-ductility of OFCs, which leads to damage-resistant material behavior and high thermal shock resistance, is not achieved by the “weak interface composite” as is the case for non-oxide ceramic composites (CMCs), but mostly by a weak matrix.<sup>17</sup> In these weak matrix composites, the crack energy dissipates due to the deflection and branching of the cracks at the pores of the porous matrix. In addition, cracks are deflected due to the point

This is an open access article under the terms of the [Creative Commons Attribution](https://creativecommons.org/licenses/by/4.0/) License, which permits use, distribution and reproduction in any medium, provided the original work is properly cited.

© 2022 The Authors. *International Journal of Applied Ceramic Technology* published by Wiley Periodicals LLC on behalf of American Ceramics Society.

contacts between the fibers and the matrix, preferably parallel to the fiber, instead of passing through the fibers.<sup>17</sup>

Due to their low drapability, cost intensive fabric reinforcements quickly reach their limits, especially when implementing complex structures with spherical geometries, narrow radii and transition areas between curved and flat surfaces. For such geometries, near-net-shape manufacturing processes such as fiber spraying, which yield drapable short fiber reinforcements, are generally more suitable. In addition, short fiber-reinforced OFCs allow a significant reduction in material costs of up to 60 % for the same fiber volume content, which depends on the filament count of the fabric or roving.<sup>18,19</sup> Currently, only a few studies<sup>20–26</sup> are known, which have already used high-performance oxide fibers such as Nextel 610 as a short fiber reinforcement in OFC.

A possible manufacturing process for short fiber reinforced OFC is ceramic injection molding.<sup>20–23</sup> Due to the process, only fiber lengths of 200–300  $\mu\text{m}$ <sup>21</sup> respectively 45–422  $\mu\text{m}$ <sup>23</sup> remain in the sintered OFC, which, as confirmed by Böttcher et al.<sup>23</sup>, unfortunately does not evoke any damage tolerant fracture behavior with the used weak matrix. An alternative route for the manufacturing of short fiber reinforced OFC is the use of binder-stabilized short fiber bundle preforms<sup>24</sup> In this process, the short fiber bundle preforms are first stabilized with a liquid binder, before they are infiltrated with a slurry, dried, and finally sintered. Short fiber bundle-reinforced OFCs (SF-OFC) produced in this way were able to exhibit a certain damage tolerant fracture behavior.<sup>24</sup> Another process for manufacturing a damage tolerant SF-OFC is oxide ceramic short fiber spraying.<sup>25,26</sup>

In the field of polymer matrix composites (PMC), fiber spraying is one of the oldest and simplest manufacturing process besides hand lamination. Due to the low investment costs, high flexibility, and cost-effectiveness even for small batch sizes, the process has been a common method for the production of large and complex components with moderate strength requirements for more than 60 years.<sup>27,28</sup> Fiber spraying is used in large scale especially for glass fiber reinforced plastics. Due to the continued importance of this manufacturing process, research continues on sprayed glass,<sup>29–54</sup> carbon,<sup>52–65</sup> or natural<sup>66–74</sup> short fiber-reinforced plastics. In this process, the fibers are cut in a cutting unit and sprayed mostly randomly or by using special fiber feed units, aligned<sup>29–34,54–58,74</sup> on a mold. Unless the fibers are hybrid fibers,<sup>29–32</sup> that is, reinforcing fibers alongside thermoplastic fibers in one roving with thermoplastic fibers serving as binding phase, the cut fibers are usually sprayed together with a resin or, for the production of preforms, with a powdered binder.<sup>55–62,65</sup> In addition to PMC, short fiber spraying processes are

also used for the production of fiber-reinforced cement components.<sup>75–77</sup>

Due to the usual manual production routes, there are sometimes strong variations in quality, which mostly limit the use of such materials to simple structures that are not exposed to heavy loads, such as molds, paneling, and tubs.<sup>27</sup> In order to enhance reproducibility and component quality, the automation of the fiber spraying process by using robots<sup>29–40,43,55–63,66,67,70,74–76</sup> has been the focus of research in the past few years. In the field of fiber-reinforced ceramics, this process is new and not yet established.

In a previous study,<sup>78</sup> a fiber spraying system with a 6-axis industrial robot for the automated manufacturing of SF-OFC was designed and built. The novel SF-OFCs exhibited in-plane isotropic material properties and a bending strength of up to  $177 \pm 16$  MPa with a strain of .39% were achieved. Importantly, the strains were in the range of continuously fiber-reinforced OFCs leading to a quasi-ductile fracture behavior, albeit at a lower strength level (bending strength fabric reinforcement:  $237 \pm 21$  MPa ( $0^\circ/90^\circ$ )<sup>9,19</sup>). But, off-axis bending strengths of the fabric-reinforced OFC were only  $69 \pm 7$  MPa,<sup>9,19</sup> which is only 40% of the bending strength of the SF-OFC.<sup>26</sup> It is important to note that in contrast to PMC, the aim is not to separate the filaments but to maintain the bundle structure as far as possible in order to achieve the required damage tolerance in CMC.<sup>9,25,26</sup>

Based on our previous studies<sup>9,19,26</sup> which have already shown that damage-tolerant SF-OFC can be manufactured via a spraying process, it was the objective of this work to deepen the understanding of this process and the material. Therefore, this work deals on the one hand with the identification of significant process parameters of the fiber spraying process, and on the other hand with a basic consideration of SF-OFC with regard to fiber orientation and length. A design of experiments (DoE) is carried out for the detection of significant process parameters. Various studies on the fiber spraying of PMCs identified the travel height,<sup>36</sup> spray angle,<sup>39</sup> and movement speed<sup>67</sup> as relevant parameters. Therefore, these factors were also investigated in this study.

## 2 | EXPERIMENTAL PROCEDURE

In this study, SF-OFCs were manufactured via an automated fiber spraying process and characterized with regard to bending strength and microstructure. The focus of the investigation was first on the identification of significant process parameters for the fiber spraying process and secondly the effect of different fiber lengths and their respective fiber orientation.

## 2.1 | Materials

The used matrix and reinforcement phases were identical to those in our previous investigation.<sup>26</sup> A low viscosity slurry with 60 wt% solid content was used for the matrix. The solid content consisted of 70 wt% sintering-sluggish alumina powder (computed tomography [CT]-3000 SG, Almatis, OYAK, Turkey) with a  $d_{50}$  of approximately .5  $\mu\text{m}$  and 30 wt% of the sintering-active powders ( $d_{50} \approx .1 \mu\text{m}$ ) 3YSZ (TZ-3Y-E, Tosoh, Japan) and alumina (Taimicron TM-DAR, Taimei Chemicals Co., Japan). Relative to the solid content, 1.5 wt% Sokalan PA15 dispersant (BASF, Germany), 26 wt% glycerol (99.5 % AnalaR NORMAPUR, VWR, Germany), and distilled water made up the liquid phase. The hygroscopic properties of the glycerol allowed the adjustment of the water content of the slurry and thus the tack of the preimpregnated fiber products (prepregs).<sup>9,10,79</sup> This tack was necessary for the subsequent lamination of the prepregs. To facilitate vacuum bagging, .5 wt% binder (PLEXTOL B 500, Synthomer plc, England) based on the total mass of the slurry was added to the slurry.

The reinforcement fibers used in this study were Nextel 610 10 000 den high purity  $\alpha$ -alumina fiber bundles (3 M Corporation, US) with polyvinyl alcohol sizing. The sizing was necessary for processing and preserving the bundle structure of the short fibers. However, the sizing did not affect the wetting behavior, which allowed the slurry to infiltrate the fiber bundle, leading to the aspired damage-tolerant behavior of the OFC.<sup>19,26</sup>

## 2.2 | Fiber spraying process

During the fiber spraying process, the slurry and cut short fiber bundles were sprayed simultaneously onto a mold. As shown in Figure 1, the central elements of the used fiber spraying system were a spray gun and a cutting unit, which together formed the tool head and were attached to a 6-axis industrial robot (TX2-90L, Stäubli International AG, Switzerland). The slurry was fed via compressed air from a pressure feeding container to the high-volume, low-pressure automatic spray gun, where it was atomized. The geometry of the slurry jet and thus the spray pattern was adjusted by round and flat jet pneumatic nozzles. The slurry flow rate was kept constant over the entire study. In the pneumatically driven cutting unit, the sized continuous fiber bundles were cut to a predefined length between a rubberised anvil roller and a cutting roller fitted with blades (Figure 1B). Depending on the used number of blades, fiber bundle lengths of 14, 28, 56 and 112 mm were realized. As for the slurry flow rate, the speed of the cutting unit and thus the mass flow of fiber material was

kept constant during the whole study. The cut fibers were ejected from the cutter and immediately carried away by the slurry jet. The fiber bundles were largely infiltrated in flight before they hit the mold layer by layer together with excess slurry.

In order to ensure a direct comparison with our previous investigations,<sup>26</sup> the OFCs were prepared in the exact same way, that is, four layers of 400 mm length were sprayed directly on top of each other to achieve sufficient specimen thickness. The used robot trajectory (linear path, traverse height, and movement speed) as well as the orientation (spray angle) of the tool head (Figure 2) was programmed via a standard program on the teach pendant of the robot. In our previous study, the standard parameter settings were fixed at a movement speed of .32 m/s, a travel height of 400 mm and at a spray angle of 65°. This parameter set enabled a dense spray pattern over a width of about 100 mm and a complete infiltration of the fiber bundles, which then resulted in a quasi-ductile fracture behavior in the SF-OFC comparable to fabric-reinforced OFC. As part of a full factorial experimental design, the standard parameter settings were altered. The travel height was set at 300 and 500 mm, whereas spray angles of 50 and 80° and a movement speed of .18 m/s were also investigated. The examinations regarding the fiber length and orientation were carried out with the standard parameter set.

Regardless of the process parameter used for spraying, all prepregs were manually precompacted using a finned roller, thereby removing entrapped air from the prepreg. The prepregs were predried for 1 h in a drying cabinet (FDL 115, Binder, Germany) at 50°C. Thereby, the binder in the slurry was activated. The prepregs were then conditioned in a climate chamber (305SB / +10 IU, Weiss, Germany) at 25°C and a humidity of 53 % to adjust the tack of the prepreg. Note that 260×100 mm<sup>2</sup> sheets were cut from the conditioned prepreg and covered on both sides with a polyethylene (PE) nonwoven without any further lamination step and pressed between two sheets in a vacuum bag. Vacuum was first drawn for 2 h at room temperature, then at 60°C in a drying cabinet for up to 12 h. After the vacuum bag was removed, the self-supporting green bodies were dried for at least 12 h at 100°C and finally sintered in a furnace (LH 60/14, Nabertherm, Germany) for 2 h at 1225°C in air.

## 2.3 | Design of experiments

A 2<sup>3</sup> full factorial experimental design, according to DoEs specifications, was set up (Table 1). The aim was not to find “the optimum parameter setting,” but rather to show tendencies in which direction parameters have to be followed more closely in order to achieve a high component

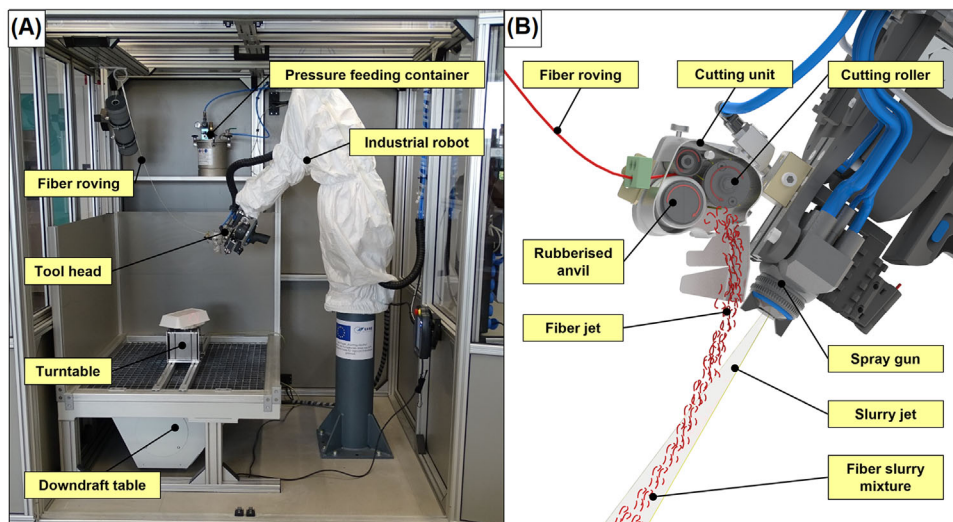


FIGURE 1 ((A) Automated fiber spraying system adapted from Winkelbauer et. al.<sup>26</sup>, (B) CAD model of the tool head

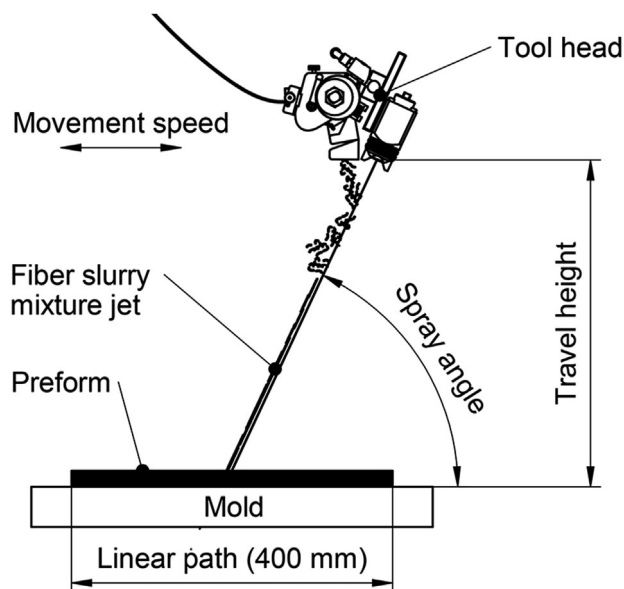


FIGURE 2 Schematic illustration of the fiber spraying process and parameter, adapted from Winkelbauer et. al.<sup>26</sup>

quality.<sup>80</sup> For a quantitative evaluation of the component quality (output), only the bending strength (response variable) was considered in this section. Examples of potential variables influencing the fiber spraying process and thus the component quality are among others travel height, movement speed, spraying angle, spraying direction, distance and angle of the cutting unit to the automatic spray gun, angle of inclination of the mold surface, or material parameters such as the material flowrate and the slurry viscosity. Within this first investigation, only the parameters travel height A, spray angle B, and movement speed C were considered as factors. As mentioned above, these

TABLE 1  $2^3$  full factorial experimental design – Factors travel height, spray angle, and movement speed

Experiment	Travel height (mm)	Spray angle (°)	Movement speed (m/s)
#1	300	50	.18
#2	300	50	.32
#3	300	80	.18
#4	300	80	.32
#5	500	50	.18
#6	500	50	.32
#7	500	80	.18
#8	500	80	.32

three factors have already been described for PMC and in the following will be examined comparatively for the oxide ceramic short fiber spray process. The current standard parameters (travel height: 400 mm, spray angle: 65°) were taken as reference points for the investigation, which were either increased (travel height: 500 mm, spray angle: 80°) or decreased (travel height: 300 mm, spray angle: 50°). Factor levels of .18 m/s and .32 m/s were considered as movement speeds. All specimens of this DoE were prepared with a fiber length of 14 mm and the same slurry composition. Experiments were performed in two blocks (experiment #1 - #4) and (experiment #5 - #8) without further randomization. Through the DoE, it was possible to analyze the effect of the individual factors on the bending strength of the specimens (15 single specimens per experiment) as well as possible interactions of the factors (AB, AC, BC, ABC).<sup>81,82</sup>

For easier interpretation, the significance test was evaluated graphically by comparing the widths of the 95 %, 99 %, and 99.9 % confidence levels with the effect of the factors and interactions. The effect of the factors was classified into nonsignificant (<95 % confidence level), low significant (between 95 % and 99 % confidence level), significant (between 99 % and 99.9 % confidence level), and highly significant (>99.9 % confidence level).<sup>82</sup>

## 2.4 | Characterization

Due to the random orientation of the fibers, it is not possible to use the same methods to determine the fiber volume content of short-fiber reinforced composites as for long-fiber composites using gravimetric via grammage or optical evaluations of microsections. Since a certain amount of the sprayed material ends up as overspray next to the specimen, it is not directly known how much fiber, or slurry is present in the specimen plate. In order to obtain an approximate value, a 100 × 30 mm strip of each green body was used to determine the fiber volume content. For this purpose, the green matrix of the strips was washed out leaving only fibers behind. These fibers were subsequently dried and weighed. From the determined fiber mass and the fiber density (3.9 g/cm<sup>3</sup>),<sup>83</sup> the fiber volume of the strip was calculated. To determine the fiber volume content of the sintered OFC, the mass of the sintered OFC plate was first weighed. This OFC plate was then trimmed using a water-cooled diamond wire saw (Type 6234, Well, Germany) after which the density and porosity were determined using Archimedes' principle. From the mass of the OFC plate (before trimming) and the density, the total volume of the OFC plate was calculated. To determine the fiber volume content, the fiber volume of the strip was finally extrapolated to the plate size of 260 × 100 mm<sup>2</sup>, and the amount of the total volume of the OFC plate was calculated. For the mechanical characterization of the specimen plate, five 50 × 10 mm<sup>2</sup> samples each were cut out in 0, 45, and 90° direction with respect to the spraying direction by the water-cooled diamond wire saw. The three-point bending test was carried out according to DIN 658-3<sup>84</sup> with a universal testing machine (inspekt 5 table blue, Hegewald & Peschke, Gemany). The strain was determined via the traverse path. This allowed a first comparison of the strains within the test series. To ensure the required standard length/thickness ratio of at least 20,<sup>84</sup> the support span had to be dynamically adjusted to the average thickness of the specimen plate according to Table 2. This was necessary because strong thickness variations between the obtained OFC plates were to be expected, particularly when investigating different movement speeds. Especially in the case of very thin specimens

TABLE 2 Support span for the bending tests

Plate thickness (mm)	Support span (mm)
<.76	15
.76–1.00	20
1.01–1.25	25
1.26–1.50	30
1.51–1.75	35
1.76–2.00	40

with a thickness of less than 1 mm, this dynamic adaptation of the supports was crucial to be able to measure the strains of the material and not only the system stiffness of the plate.

The microstructure of each composite was analyzed using a scanning electron microscope (SEM, Zeiss Sigma 300 VB, Zeiss, Germany). Specimens of each OFC were cut from the center of the plate by using the water-cooled diamond wire saw, embedded in epoxy resin, ground, and polished. Before analyzing the specimens in the SEM, the epoxy resin was burnt out at 700°C, and the specimens were sputtered at a pressure of .1 mbar and a voltage of 30 mA for 2 min with gold by a sputter coater (108auto, Cressington Scientific Instruments UK, UK).

In sintered OFC, it is not possible to determine the fiber orientation without complex and cost-intensive micro-CT ( $\mu$ -CT).<sup>29</sup> Due to a thin matrix film on the surface, the orientation on the surface cannot be analyzed optically either, as is for example the case for the optical measurements of dry fiber semifinished products of glass fiber rovings with thermoplastic yarn as binder.<sup>32–34</sup> Therefore, as in our previous study,<sup>26</sup> a single layer of fibers and slurry was sprayed onto a transparent plastic film with the same settings of the respective sprayed OFC plate. After drying at room temperature, this single layer was photographed on a transmitted light table. Three fields with a size of 110 × 70 mm<sup>2</sup> were photographed and evaluated by the open-source software ImageJ. With the OrientationJ plugin, it was possible to create a histogram that showed the amount of fibers as a function of the orientation (−90° to +90°). An average distribution was calculated from the three resulting histograms of each single layer.

## 3 | RESULTS AND DISCUSSION

### 3.1 | Process parameters

The result of the significance test of the effect of the factors travel height, spray angle, and movement speed on the bending strength is presented in Figure 3. The travel height

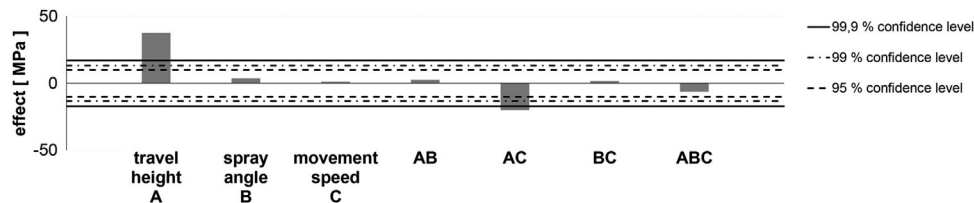


FIGURE 3 Graphical illustration of the significance test

TABLE 3 Summary of the factors travel height (A), spray angle (B) and movement speed (C) with the corresponding interactions, the resulting response variable, that is, the bending strength and the average plate thicknesses with correspondingly used support spans

Experiment	Factors			Interactions				Response variable	
	Travel height (mm) A	Spray angle (°) B	Movement speed (m/s) C	AB	AC	BC	ABC	Bending strength (MPa)	Plate thickness (support span) (mm)
#1	300 (-)	50 (-)	.18 (-)	+	+	+	-	86 ± 19	1.47 (30)
#2	300 (-)	50 (-)	.32 (+)	+	-	-	+	99 ± 25	.92 (20)
#3	300 (-)	80 (+)	.18 (-)	-	+	-	+	79 ± 24	1.57 (35)
#4	300 (-)	80 (+)	.32 (+)	-	-	+	-	108 ± 39	.97 (20)
#5	500 (+)	50 (-)	.18 (-)	-	-	+	+	135 ± 18	1.12 (25)
#6	500 (+)	50 (-)	.32 (+)	-	+	-	-	120 ± 30	.54 (15)
#7	500 (+)	80 (+)	.18 (-)	+	-	-	-	145 ± 29	1.11 (25)
#8	500 (+)	80 (+)	.32 (+)	+	+	+	+	121 ± 32	.69 (15)

(A) exceeded the solid line limit of the 99.9 % confidence level and is therefore considered highly significant. In addition, the graph shows a highly negative significance of the interaction between travel height and movement speed (AC). Therefore, from now on, both factors must always be considered together. All other factors and interactions were not significant and had therefore no considerable influence on the bending strength of the composite. Compared with observations from the field of PMC, similar independence of the material strength from the movement speed and the spray angle were reported. For fiber spraying of pineapple fiber-reinforced vinyl ester, Hanafee et al.<sup>67</sup> detected only a significance of the speed on the mass flowrate of the resin as well as a slight influence on the fiber orientation. With regard to tensile and bending strength, an optimum setting for the highest possible strength values was found in their investigation. Based on the values given, however, it was not possible to derive a direct correlation between the movement speed and the component strength, either. Additionally, in an investigation of sprayed glass-fiber reinforced polyurethane<sup>39</sup>, no significance of the spray head orientation on the mechanical properties of the composites was found.

In order to illustrate the results from the DoE in more detail, Table 3 shows the eight factor level combinations, their interactions and the resulting average bending strengths determined at an angle of 0, 45, and 90°

relative to the spraying direction. The levels of the interactions were determined by multiplying the coded levels of the input factors (positive or negative) acting in the interaction.

At a low travel height (experiment #1 - #4), average bending strengths between 79 ± 24 MPa and 108 ± 39 MPa were achieved. However, spraying at a distance of 500 mm (experiment #5 - #8) resulted in much higher bending strengths between 120 ± 30 MPa and 145 ± 29 MPa. The full factorial experimental design demonstrates that the bending strength and hence the component performance generally improve with increasing travel height. This indicates that the fiber bundles need a minimum flight length in the atomized slurry jet in order to be infiltrated sufficiently, and therefore a minimum travel height is necessary. Insufficient infiltration of the fiber bundles leads to a strength decrease and loss of the damage-tolerant fracture behavior. The SEM images in Figure 4 provide the microstructures of experiment #3 and #7, which were fabricated with a spray angle of 80°, a movement speed of .18 m/s and travel heights of 300 mm (Figure 4A) and 500 mm (Figure 4B), respectively. At this point, it should be mentioned once again that the sprayed preforms were identically vented and compacted after the spraying process was completed. It can be seen that if the distance was too small (Figure 4A), pores in the fiber bundles were visible, which was attributed to insufficient infiltration of

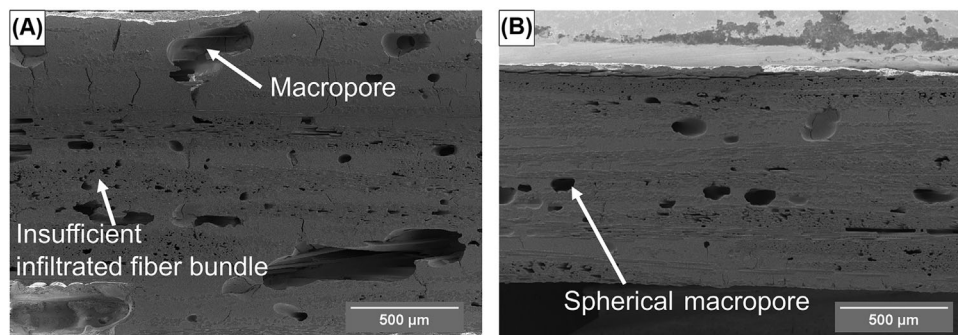


**FIGURE 4** Scanning electron microscope (SEM)-images of the microstructure of sprayed 14 mm short fiber bundle-reinforced oxide fiber composites (SF-OFC) with a travel height of (A) 300 mm (experiment #3) and (B) 500 mm (experiment #7)

the fiber bundles. Overall, the microstructure (Figure 4A) of this specimen is considerably more porous (porosity: 44 vol%) than that of the specimen produced with an increased travel height (porosity: 37 vol%). The macropores of the specimen from experiment #3 were also significantly larger and more elongated, which tended to be more critical in terms of specimen strength than spherical pores as in specimen, which were sprayed with a travel height of 500 mm (Figure 4B). This correlation between pore shape and specimen strength was already observed by Puchas et al.<sup>8,10</sup>

In the fiber spraying process, the fiber bundles were distributed homogeneously in the slurry jet without losing their bundle structure. A lower distance between the spray gun and the mold surface leads to a distribution of the fiber bundles over a small area and therefore an accumulation on the mold. It was subsequently difficult to remove the air from these accumulations resulting in macroporous OFCs with low strengths. Additionally, the fiber bundle infiltration was, as already mentioned, insufficient due to the short flight length. By increasing the distance between the spray gun and the mold, the fiber bundles had more time for distribution in the slurry jet and were therefore applied more homogeneously on the mold. Subsequently, it was possible to compact these sprayed layers better than the previously mentioned fiber accumulations. Moreover, the infiltration of the fiber bundles was also more sufficient. The resulting microstructure therefore appears more homogeneous and less macroporous. The obtained results are in good agreement with a previous study of Jeon et al.,<sup>36</sup> who also identified a correlation between material application and spray height for glass fiber reinforced polydicyclopentadiene. The higher the spray height, the more even was the fiber distribution, although this phenomenon was more pronounced with longer fibers (50 mm).

Due to the marked significance of the interaction between the travel height and movement speed, it is not sufficient to consider only the travel height. It should be noted that the bending strength of the experiments with

500 mm travel height increased during the transition from the high (+) to the low level (–) of the interaction AC (travel height and movement speed). Considering experiments #5, #6, and #7, for example, it can be seen that with a decreasing movement speed the strength increased from  $120 \pm 30$  MPa (#6) to  $135 \pm 18$  MPa (#5), and  $145 \pm 29$  MPa (#7) regardless of the spray angle. Correspondingly, in the experiments with low travel heights (experiments #1 - #4), a faster movement speed resulted in an improved bending strength. This can be seen by comparing experiment #3 ( $79 \pm 24$  MPa) with experiment #2 ( $99 \pm 25$  MPa) or experiment #4 ( $108 \pm 39$  MPa).

The slower the spraying device moves over the component, the higher was the material application on the mold. To be able to deaerate and compact the preform sufficiently, material accumulations have to be prevented by faster movement speeds at low travel heights. A high distance between the spray gun and the mold leads to a larger fanning out of the fibers in the slurry jet and consequently to the deposition of a thin layer. In order to ensure the application of sufficient material on the mold, the movement must be executed more slowly. It can be concluded that at a low travel height (300 mm), the movement should be faster (.32 m/s), and at a higher travel height (500 mm), the movement should be slower (.18 m/s).

### 3.2 | Fiber length

In this test series, the fiber lengths 14, 28, 56, and 112 mm were considered. The mean bending strengths, strains, and Young's modulus of 15 individual specimens (average of five specimens each in 0, 45, and 90° test orientation) are given in Table 4 together with the corresponding porosity. The average fiber volume content of the four specimen plates was approximately 29 vol%. Representative stress-strain curves are shown in Figure 5. The stress-strain curves indicate that all specimens exhibited a strikingly damage-tolerant fracture behavior due to

**TABLE 4** Bending strengths, strains, Young's modulus, porosities, and the average plate thicknesses with correspondingly used support spans of sprayed short fiber bundle-reinforced oxide fiber composites (OFCs) with different fiber lengths and an average fiber volume content of 29 vol%

	Bending strength (MPa)	Strain (%)	Young's modulus (GPa)	Porosity (vol%)	Plate thickness (support span) (mm)
14 mm short fibers	133 ± 27	.56 ± .10	29 ± 7	40	.71 (15)
28 mm short fibers	141 ± 27	.57 ± .09	30 ± 4	41	.95 (20)
56 mm short fibers	148 ± 36	.61 ± .11	30 ± 7	35	.84 (20)
112 mm short fibers	163 ± 29	.64 ± .13	35 ± 7	38	.98 (20)

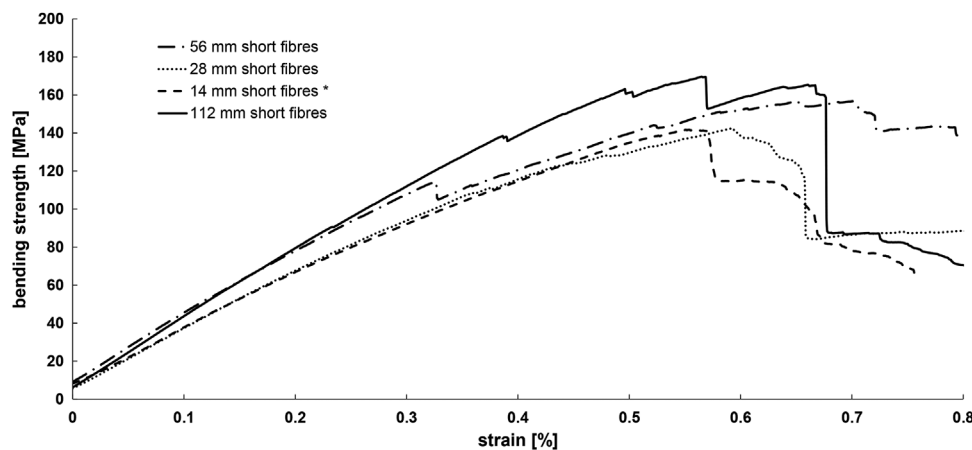


**FIGURE 5** Representative stress-strain curves of sprayed short fiber bundle-reinforced oxide fiber composites (OFCs) with different fiber lengths (\*14 mm short fiber bundle-reinforced OFC were already described in a previous study<sup>26</sup>)

their fiber reinforcement. Accordingly, they did not fail catastrophically after reaching maximum strength.

Considering the strains, a slight improvement from  $.56 \pm .10$  % for 14 mm short fibers to  $.64 \pm .13$  % for 112 mm short fibers was seen with increasing fiber lengths. These results are consistent with observations made in a previous study<sup>26</sup> on hand-laid unidirectional specimens. An occurring crack is therefore deflected along an increasingly longer fiber, and its energy is dissipated over a longer path. While the strains of the unidirectional, hand-laid OFCs with isolated fibers were on average  $.20 \pm .03$  %<sup>26</sup> (14 mm short fiber) and  $.22 \pm .03$  %<sup>26</sup> (28 mm short fiber), strains of  $.56 \pm .10$  % (14 mm short fiber), and  $.57 \pm .09$  % (28 mm short fiber), respectively, were achieved by the random orientation of the sprayed specimens in our present study. Therefore, it can be concluded that the influence of the random arrangement of the fiber bundles and the preservation of the bundle structure is much more important than the influence of the fiber length.

The fiber length also influenced the Young's modulus of the SF-OFC. While the Young's modulus remained almost constant up to a fiber length of 56 mm (approx. 30 GPa), it increased slightly to  $35 \pm 7$  GPa at a fiber length of

112 mm. Figure 5 also shows that the linear-elastic region of specimens with 112mm fiber reinforcement was more pronounced than that of specimens with shorter fiber lengths. These samples can thus potentially loaded reversibly over a longer range. However, since the strain was only determined over the traverse path in this investigation, the results of the strain and Young's modulus are not to be considered as a highly accurate material parameter, but only as a comparative value within this series of tests. A validated study using video or laser extensometers is forthcoming.

Multiple intersections of the randomly oriented short fiber bundles lead to an increasingly extensive deflection and branching of the cracks in the random fiber architecture. The presence of fiber bundles instead of isolated fibers delays the propagation of cracks. Levi et al.<sup>85</sup> described that fiber cracks initially occur randomly after the formation of cracks in the porous matrix. Subsequently the failure of multiple fibers within a bundle leads to fiber bundle failure. The ultimate failure of the composite finally occurs after the connection of multiple fiber bundle cracks through the intervening matrix regions. If this bundle structure is missing as in the case of the hand-laid OFC,<sup>26</sup> crack formation cannot be delayed, and the crack propagates unhindered through the matrix areas.

All these phenomena ultimately lead to a quasi-ductile fracture behavior and to strains comparable to those of conventional fabric-reinforced OFCs (average .4 %), from our previous study.<sup>9</sup>

Kuppinger et al.<sup>38</sup> described an increasing number of pores and cavities for glass fiber-reinforced polyurethanes composite with increasing fiber length, due to increased intersections of the fibers. Considering the porosities in Table 4, such a correlation between fiber length and porosity was not detected. These differences in porosity were caused by the different levels of densification. During the production of the glass fiber reinforced polyurethane composites, the sprayed semi-finished product with a plate thickness of approximately 4 mm was not compressed. By contrast, in the fiber spraying process in this study, much thinner (approximately 1 mm) and thus better compactable semi-finished products were first precompact and vented manually using a finned roller before they were pressed via vacuum bagging. The occurring variations in porosity seen in this study can be attributed primarily to the manual precompacting and venting step.

In the field of fiber sprayed PMCs, the increase of mechanical properties with increasing fiber length cannot be assumed as a general rule. While Jeon et al.<sup>36</sup> were able to demonstrate higher tensile (increase of up to 20 %) and bending strengths (increase of up to 30 %) with 50 mm fiber length instead of using 25 mm fibers, Kuppinger et al.<sup>38</sup> were unable to demonstrate any significance of the fiber length (6 and 12 mm fibers) on the bending and tensile properties.

Considering the bending strength values of the SF-OFC specimens with 14 mm ( $133 \pm 27$  MPa), 28 mm ( $141 \pm 27$  MPa), 56 mm ( $148 \pm 36$  MPa), and 112 mm ( $163 \pm 29$  MPa) fiber length, it can be seen that with an increasing fiber length, the bending strength of the SF-OFCs increased substantially. This was in excellent agreement with the results of the hand-laid specimens in our previous study,<sup>26</sup> albeit the differences for the sprayed specimen were less pronounced. This is due to the fact that the fiber sprayed specimens have a random fiber orientation, whereas all fibers of the hand laid specimens were oriented in loading direction. Consequently, not all fibers contributed to the reinforcement of the composite in the load direction, which significantly reduces their effect.

### 3.3 | Fiber orientation

Figure 6 shows the average bending strengths from Table 4 separated into the three testing directions 0, 45, and 90°. Except for a fiber length of 56 mm in 90° direction, no significant differences between the three testing directions were detected for the investigated fiber lengths. While

the bending strengths of 14 mm SF-OFC varied between  $126 \pm 34$  MPa (45°) and  $144 \pm 31$  MPa (90°), that of 112 mm SF-OFCs varied between  $157 \pm 19$  MPa (90°) and  $172 \pm 37$  MPa (0°).

While the bending strength decreases in the 90° direction for the OFCs with 56 mm fiber length, only a small difference of maximum four percentage points (0° to 90° fiber orientation) was detected during the optical analysis of a single layer via ImageJ (Figure 7C). In the optical analysis of the fiber orientation in our previous investigation,<sup>26</sup> the average distribution of the specimens with a fiber length of 14 mm (Figure 7A) already showed a slightly preferred orientation in the 0° direction. A similar increase was seen in the fiber lengths examined in this study (Figure 7) as well. The minimal preferred fiber orientation in the spray direction (0°) can be explained by the air stream with which the fibers are conveyed from the cutting unit. However, this partially existing fiber orientation was largely cancelled out when the fibers hit the atomized slurry jet, whereby the fiber bundles distribute and orient themselves randomly in the slurry jet. In general, it should be expected that longer fibers are more likely to be oriented in the direction of the spray as they pass through the fiber outlet of the cutting unit, as has been demonstrated specifically by Harper et al.<sup>58</sup> This increase could not be verified based on the optical evaluation in this study. However, the supposed preferred orientations were only confirmed by the bending strength values in Figure 6 for the SF-OFCs with 112-mm fiber length. Therefore, it is doubtful whether a share of up to 10 % oriented in the direction of  $-5^\circ$  to  $5^\circ$  can be considered as a preferred orientation. In further investigations, it has to be determined above which proportion of fibers in the loading direction the mechanical properties are significantly influenced. In our previous study,<sup>26</sup> the strong deviation of the bending strengths of sprayed SF-OFC was already noted. This strong deviation was explained by the small specimen thickness and the locally varying fiber volume contents and fiber orientations in the loaded volume. Considering the standard deviation, the respective bending strengths of the four investigated fiber lengths can also be regarded as more or less similar, regardless of the test direction. Thus, the material can be described as in-plane isotropic.

The in-plane isotropic material behavior occurs automatically during the applied process. Whereas various systems<sup>29–34,54–58,74</sup> were previously described using a specially designed cutting unit with a fiber guidance unit to create an aligned fiber orientation, in this study a basic fiber spraying system without manipulators was used. The fibers were ejected from the cutting unit by an air stream and directly carried away by the slurry jet. The fiber bundles thus underwent a change in direction as well as spreading and random distribution over the width of the

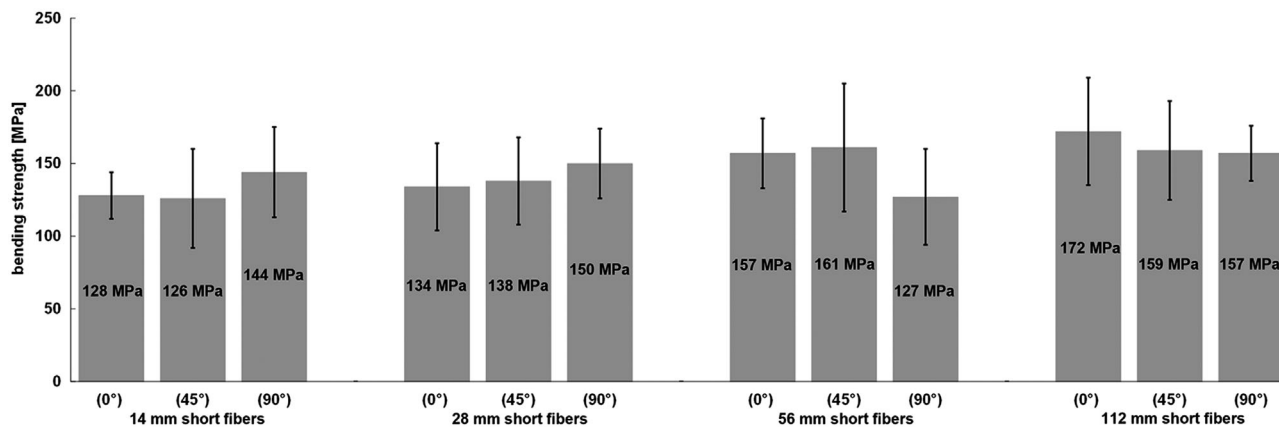


FIGURE 6 Comparison of the bending strengths of sprayed short fiber bundle-reinforced oxide fiber composites (OFCs) with different fiber lengths, divided into the three testing directions 0°, 45°, and 90°, relative to the spray direction

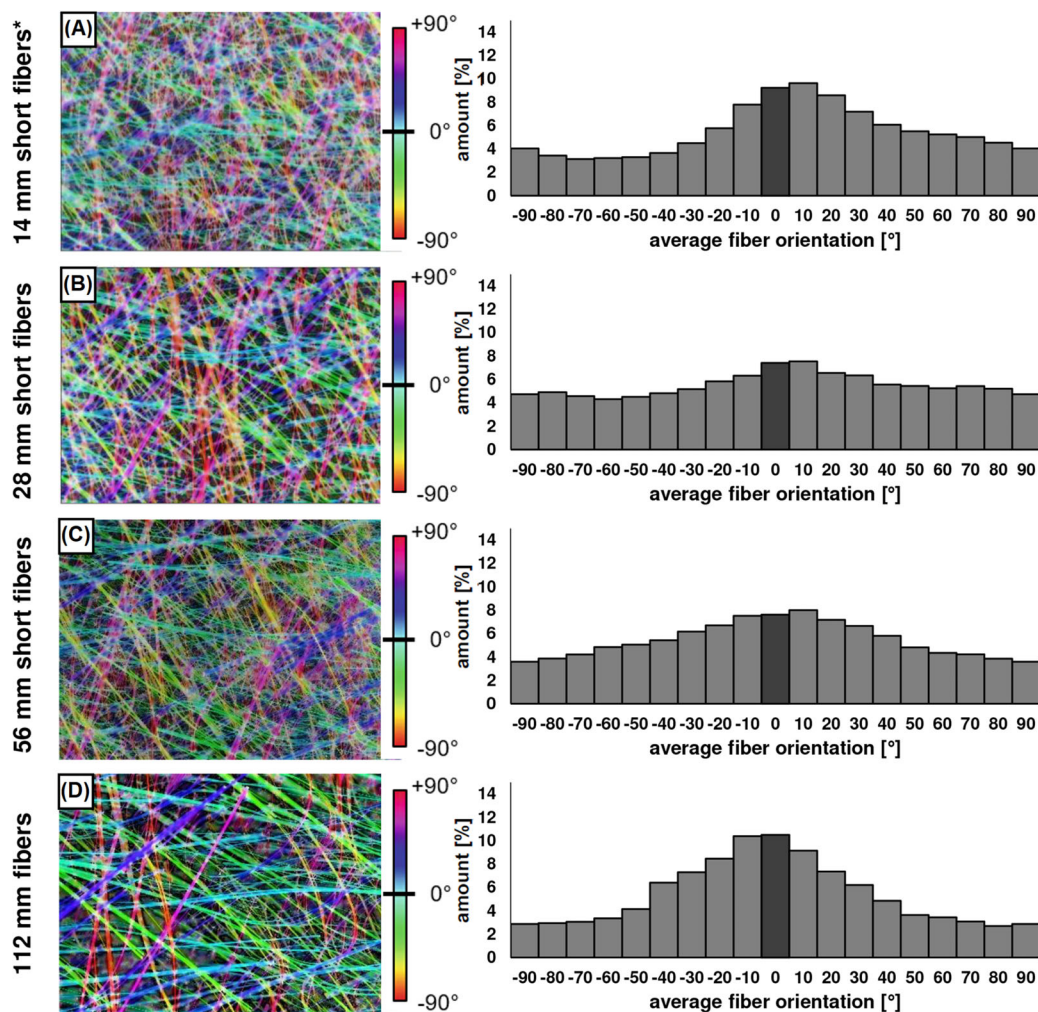


FIGURE 7 Representative single layers analyzed via ImageJ and the average distribution curve of the fiber orientations of (A) 14 mm short fibers, (B) 28 mm short fibers, (C) 56 mm short fibers, (D) 112 mm short fibers (\*14 mm short fiber bundle-reinforced oxide fiber composites (OFCs) were described in a previous study<sup>26</sup>)

slurry jet. Due to this random orientation of the fiber bundles in the slurry jet, which was also not changed by the impact on the mold surface, an in-plane isotropic property profile was achieved in the final SF-OFCs. This in-plane isotropy is independent of the fiber length. Kuppinger et al.<sup>39</sup> obtained the same result when investigating the influence of 6 and 12 mm glass fibers on the fiber orientation in fiber-reinforced polyurethanes. The random orientation was also explained by the pneumatic transport of the fibers to the spraying head and into the polyurethane spray as well as turbulences in the transport pipe and in the mixing head. In addition, it was described that the orientation was not influenced by the exit of the cut fibers out of the spray head and the impact on the mold surface.<sup>39</sup>

## 4 | CONCLUSIONS

An automated fiber spraying process was developed, and the novel short fiber bundle-reinforced OFCs material was investigated with regard to fiber length and orientation. In the field of PMCs, short fiber spraying is one of the most common processes for the production of large components with moderate strength requirements. Within this study, the manufacturing concept was transferred to OFC. It was shown that there are some parallels between the fiber spraying of PMC and OFC. However, it was not possible to directly adopt the material behavior of OFCs, despite the also fiber-dominated behavior and a thorough investigation of the process-microstructure-property correlations was required. Initially, the significance of the process parameters travel height, spray angle, and movement speed on the bending strength of the SF-OFCs was investigated. The travel height and the interaction between travel height and movement speed were shown to be highly significant. To achieve the highest strength, the movement should be faster at a lower travel height and slower at a higher travel height. The investigation of fiber length and orientation was performed on sprayed SF-OFCs with fiber lengths of 14, 28, 56, and 112 mm, respectively. All tested specimens showed a quasi-ductile fracture behavior. With increasing fiber length, the bending strength increased from  $133 \pm 27$  MPa with 14 mm fiber reinforcements to an average of  $163 \pm 29$  MPa with 112 mm fibers. The bending strengths are therefore below the strength values of fabric-reinforced OFC in the main loading direction ( $237 \pm 21$  MPa at 28 vol% FVG),<sup>9,19</sup> but considerably higher off-axis properties were achieved ( $69 \pm 7$  MPa at 28 vol% FVG).<sup>9,19</sup> The strains were in the range of .6 %, which exceeded the strain of continuous fabric-reinforced OFC (.4 %).<sup>9</sup> In contrast to fabric reinforcements, SF-OFCs did not show any preferred orientation, regardless of the fiber length. Due to the process, the fiber-bundles were oriented randomly in the composite and led to an in-plane isotropic

property profile of the OFCs. This novel material is therefore a promising, cost-efficient material (up to 60 % cost reduction compared to fabric reinforcement)<sup>18,19</sup> for complex components for high temperature applications such as foundry, furnace construction or chemical industries.

## ACKNOWLEDGMENT

The authors gratefully acknowledge Dominik Henrich and Edgar Schmidt from the Chair for Robotics and Embedded Systems (University of Bayreuth) for enabling the automation of the short fiber spraying process.

Open access funding enabled and organized by Projekt DEAL.

## CONFLICT OF INTEREST

The authors declare that there is no conflict of interest that could be perceived as prejudicing the impartiality of the research reported.

## ORCID

Jonas Winkelbauer  <https://orcid.org/0000-0002-4805-4601>

Stefan Schafföner  <https://orcid.org/0000-0002-6526-2496>

## REFERENCES

- Wilson D, Visser L. High performance oxide fibers for metal and ceramic composites. *Composites, Part A*. 2001;32(8):1143–53.
- Ferraris M, De la Pierre S, Akram Y, Steinborn C, Puchas G, Krenkel W. High temperature creep behaviour of glass-ceramic joined Nextel 610™/Al<sub>2</sub>O<sub>3</sub>-ZrO<sub>2</sub> composites. *J Eur Ceram Soc*. 2022;42(12):5029–34.
- Jiang R, Sun X, Liu H, Liu Y, Mao W. Microstructure and mechanical properties improvement of the Nextel™ 610 fiber reinforced alumina composite. *J Eur Ceram Soc*. 2021;41(10):5394–9.
- Pritzkow WE, Wehner F, Koch D. Oxide fiber reinforced oxide ceramic matrix composite – an alternative to metallic alloys at high temperature. *Encyclopedia of materials: metals and alloys*. Amsterdam, Netherlands: Elsevier; 2022. p. 425–41.
- Simon RA, Danzer R. Oxide fiber composites with promising properties for High-temperature structural applications. *Adv Eng Mater*. 2006;8(11):1129–34.
- Guglielmi PO, Nunes GF, Hablitzel M, Hotza D, Janssen R. Production of oxide ceramic matrix composites by a prepreg technique. *Mater Sci Forum*. 2012;727–8:556–61.
- Guglielmi PO, Blaese D, Hablitzel MP, Nunes GF, Lauth VR, Hotza D, et al. Microstructure and flexural properties of multilayered fiber-reinforced oxide composites fabricated by a novel lamination route. *Ceram Int*. 2015;41(6):7836–46.
- Puchas G, Held A, Krenkel W. Near-net shape manufacture process for oxide fiber composites (OFC). *Mater Today: Proc*. 2019;16:49–58.
- Puchas G, Krenkel W. Neuartige Herstellungsverfahren für oxidkeramische Faserverbundwerkstoffe (Novel manufacturing processes for oxide ceramic fiber composites). In: *dIALOG Materialwissenschaft und Werkstofftechnik*. 2018;(1):34–41.

10. Puchas G, Möckel S, Krenkel W. Novel prepreg manufacturing process for oxide fiber composites. *J Eur Ceram Soc.* 2020;40(15):5930–41.
11. Ben Ramdane C, Julian-Jankowiak A, Valle R, Renollet Y, Parlier M, Martin E, et al. Microstructure and mechanical behaviour of a Nextel™610/alumina weak matrix composite subjected to tensile and compressive loadings. *J Eur Ceram Soc.* 2017;37(8):2919–32.
12. Almeida RSM, Pereira TFS, Tushtev K, Rezwan K. Obtaining complex-shaped oxide ceramic composites via ionotropic gelation. *J Am Ceramic Soc.* 2019;102(1):53–7.
13. Wamser T, Scheler S, Martin B, Krenkel W. Novel oxide fiber composites by freeze casting. *J Eur Ceram Soc.* 2014;34(15):3827–33.
14. Levi CG, Yang JY, Dalglish BJ, Zok FW, Evans AG. Processing and performance of an all-oxide ceramic composite. *J Am Ceramic Soc.* 1998;81(8):2077–86.
15. Radsick T, Saruhan B, Schneider H. Damage tolerant oxide/oxide fiber laminate composites. *J Eur Ceram Soc.* 2000;20(5):545–50.
16. Pritzkow WE, Almeida RS, Mateus LB, Tushtev K, Rezwan K. All-oxide ceramic matrix composites (OCMC) based on low cost 3M Nextel™ 610 fabrics. *J Euro-pean Ceramic Soc.* 2021;41(5):3177–87.
17. Zok FW. Developments in oxide fiber composites. *J Am Ceramic Soc.* 2006;89(11):3309–24.
18. Lincoln J, Jackson B, Barnes A, Beaber A, Visser L. Oxide-oxide ceramic matrix composites-enabling widespread industry adoption. *Advances in high temperature ceramic matrix composites and materials for sustainable development.* *Ceram Trans.* 2017; 263:401–12.
19. Krenkel W, Flauder S, Puchas G. Short fiber ceramic matrix composites (SF-CMCs). *Encyclopedia of materials: technical ceramics and glasses.* Amsterdam, Netherlands: Elsevier; 2021. p. 260–76.
20. Tülümen M, Hanemann T, Hoffmann MJ, Oberacker R, Piotter V. Process development for the ceramic injection molding of oxide chopped fiber reinforced aluminum oxide. *Key Eng Mater.* 2017;742:231–7.
21. Tülümen HM, Hanemann T, Piotter V, Stenzel D. Investigation of feedstock preparation for injection molding of oxide-oxide ceramic composites. *J Manuf Mater Process.* 2019;3(1): 9.
22. Piotter V, Tueluemen M, Hanemann T, Hoffmann MJ, Ehreiser B. Powder injection molding of oxide ceramic CMC. *Key Eng Mater.* 2019;809:148–52.
23. Böttcher M, Nestler D, Stiller J, Kroll L. Injection moulding of oxide ceramic matrix composites: comparing two feedstocks. *Key Eng Mater.* 2019;809:140–7.
24. Wamser T, Scheler S, Krenkel W. Method for the production of an oxide ceramic composite material and fiber preform. Munich, Germany. European Patent 2 848 599 B1. 2019.
25. Knohl S, Krenkel W, Martin B, Wamser T. Method for the preparation of an intermediate product for the manufacture of a fibre-reinforced part and device for carrying out same. Munich, Germany. European Patent 3 450 128 A1. 2021.
26. Winkelbauer J, Puchas G, Schafföner S, Krenkel W. Short fiber-reinforced oxide fiber composites. *Int J Appl Ceramic Technol.* 2022;19(2):1136–47.
27. AVK - Industrievereinigung Verstärkte Kunststoffe e. V. Handlaminieren/Faserspritzen (hand lay-up/fiber spraying). *Handbuch Faserverbundkunststoffe/Composites: Grundlagen, Verarbeitung, Anwendungen (Handbook of fiber reinforced plastics/composites: fundamentals, processing, applications).* 4th ed. Wiesbaden: Springer Fachmedien Wiesbaden; 2013. p. 326–46.
28. Ehrenstein GW. Tabellen (tables). *Faserverbund-Kunststoffe: Werkstoffe - Verarbeitung - Eigenschaften (fiber reinforced plastics: materials - processing - properties).* 2nd ed. München, Wien: Hanser; 2006. p. 282–4.
29. Michaeli W, Pöhler M. 3D-Faserspritzen mit Faserorientierung (3d fiber spraying with fiber orientation). *Lightweight Des.* 2010;3(6):57–62.
30. Hopmann C, Böttcher A. Variotherme Direktverarbeitung von thermoplastischen FVK (variothermal direct processing of thermoplastic FRP). *Lightweight Des.* 2013;6(5):44–9.
31. Hopmann C, Engelmann C, Böttcher A, Riedel R, Beste C, van der Straeten K, et al. Neue Gestaltungsmöglichkeiten thermoplastischer FVK-Leichtbauteile (novel design options for thermoplastic FRP lightweight components). *Lightweight Des.* 2015;8(3):40–7.
32. Hopmann C, Magura N, Stender S, Schneider D, Fischer K, Weg S. Establishment of an inline quality assurance method for fiber sprayed preforms. *SAMPE 2019-Charlotte, NC, May 2019, 2019.*
33. Emonts M, Fischer K, Stender S, Magura N. Self-regulated production of an automotive composite floor pan. In: *Self-regulated production of an automotive composite floor pan.* *SAMPE; May 20–23, 2019; Charlotte, NC.*
34. Stender S, Magura N, Fischer K, Emonts M. Function-orientated production of FRP components. *Lightweight Des Worldw.* 2019;12(1):18–25.
35. Hufenbach W, Fischer W-J, Gude M, Geller S, Tyczynski T. Processing studies for the development of a manufacture process for intelligent lightweight structures with integrated sensor systems and adapted electronics. *Procedia Mater Sci.* 2013;2: 74–82.
36. Jeon JH, Yoon CK, Park SH, Lee WI, Kim SM. Assessment of long fiber Spray-up molding of chopped glass fiber reinforced polydicyclopentadiene composites. *Fibers Polym.* 2020;21(5):1134–41.
37. Renkl J, Fries E. Schicht für Schicht zum hochwertigen bauteil (layer by layer to a high-quality component). *Lightweight Des.* 2010;3(4):a55–8.
38. Kuppinger J, Wafzig F, Henning F, Weidenmann KA. Influence of fibre length and concentration on the mechanical properties of long glass fibre reinforced polyurethane. *J Plastics Technol.* 2010;5:205–27.
39. Kuppinger J, Wafzig F, Henning F, Weidenmann KA, Haspel B, Elsner P. Influence of processing conditions, fiber contents and fiber lengths on fiber orientation in the polyurethane fiber spraying process. *J Plastics Technol.* 2011;6:44–65.
40. Gumerov IF, Gumerov AF, Lakhno AV, Shafigullin LN, Yurasov SY, Shafigullina GR. Glass-filled polyurethane materials produced by fiber composite spraying. *Russ Engin Res.* 2017;37(10):925–8.
41. Bobovich BB. Use of glass roving for the production of reinforced polymer composite materials by spraying. *Glass Ceram.* 2015;72(1–2):32–4.

42. Kikuchi T, Suzuki E, Zhang Y, Takai Y, Goto A, Hamada H. Effects of quantified instructional tool on spray-up fabrication method. In: Duffy VG, editor. Digital human modeling. Applications in health, safety, ergonomics and risk management: human modeling. Cham: Springer International Publishing; 2015. p. 104–13.
43. Seidlitz H, Kreuziger R. Lösungsmittelfreie PU-Mehrkomponenten Sprühtechnologie: Abschlussbericht über ein Entwicklungsprojekt (solvent-free PU multi-component spray technology: final report on a development project), funded under Ref: 24730 by the Deutsche Bundesstiftung Umwelt. Kitzscher, Germany: Lätzsch GmbH Kunststoffverarbeitung; 2008.
44. Ha SK, Na S, Bang YK, Lee HK. An experimental study on sag-resistance ability and applicability of sprayed FRP system on vertical and overhead concrete surfaces. *Mater Struct*. 2015;48(1–2):21–33.
45. Ha SK, Na S, Lee HK. Bond characteristics of sprayed FRP composites bonded to concrete substrate considering various concrete surface conditions. *Compos Struct*. 2013;100:270–9.
46. Xiao B, Yang Y, Wu X, Liao M, Nishida R, Hamada H. Hybrid laminated composites molded by spray lay-up process. *Fibers Polym*. 2015;16(8):1759–65.
47. Gude M, Fischer W-J. Großserienfähige Fertigungstechnologien für Glasfaser- Polyurethan-Verbundstrukturen mit integrierten piezokeramischen Sensorelementen und angepasster Auswertelektronik (high-volume production technologies for glass-fiber polyurethane composite structures with integrated piezoceramic sensor elements and adapted evaluation electronics). [https://www.pt-piesa.tu-chemnitz.de/P\\_3/teilprojekte/b06.php](https://www.pt-piesa.tu-chemnitz.de/P_3/teilprojekte/b06.php) Accessed 10 April 2022
48. Weder A, Geller S, Heinig A, Tyczynski T, Hufenbach W, Fischer W-J. Integration of piezoceramic sensor elements and electronic components in glass fibre reinforced polyurethane composite structures. *Procedia Eng*. 2012;47:354–7.
49. Lee HK. Effectiveness of anchorage in concrete beams retrofitted with sprayed fiber-reinforced polymers. *J Reinf Plast Compos*. 2004;23(12):1285–300.
50. Banthia N, Boyd AJ. Sprayed fibre-reinforced polymers for repairs. *Can J Civ Eng*. 2000;27(5):907–15.
51. Boyd AJ. Rehabilitation of reinforced concrete beams with sprayed glass fiber reinforced polymers. BC, Canada: University of British Columbia; 2000.
52. Lee KS. Experimental study on sprayed FRP system for strengthening reinforced concrete beams. *Adv Mater Res*. 2012;10(6):219–30.
53. Furuta T, Kanakubo T, Nemoto T, Takahashi K, Itoh K, Minamihara H. Sprayed-up FRP strengthening for reinforced concrete beams. In: International Conference on Composites in Infrastructure; June 2002; CD-ROM No. 094.
54. Jameson N. Production of aligned short-fibre composites. Birmingham, UK: University of Birmingham, 2014.
55. Harper LT, Dodworth A, Luchoo R, Warrior NR. Automated spray deposition for net-shape carbon/epoxy compression moulding. In: Proceedings of 17th International Conference on Composite Materials (ICCM-17); July 27–31, 2009; Edinburgh, UK.
56. Harper L, Turner T, Warrior N, Rudd C. Automated preform manufacture for affordable lightweight body structures. In: 26th International SAMPE Europe Conference; 2005; Paris, France.
57. Harper LT, Turner TA, Warrior NA, Rudd CD. Characterisation of random carbon fibre composites from a directed fibre preforming process: the effect of tow filamentisation. *Composites, Part A*. 2007;38(3):755–70.
58. Harper LT, Turner TA, Martin J, Warrior NA. Fiber alignment in directed carbon fiber preforms - a feasibility study. *J Compos Mater*. 2009;43(1):57–74.
59. Turner TA, Harper LT, Warrior NA, Rudd CD. Low-cost carbon-fibre-based automotive body panel systems: a performance and manufacturing cost comparison. *Proc Inst Mech Eng Part D J Automob Eng*. 2008;222(1):53–63.
60. Harper LT, Turner TA, Warrior NA, Dahl JS, Rudd CD. Characterisation of random carbon fibre composites from a directed fibre preforming process: analysis of microstructural parameters. *Composites, Part A*. 2006;37(11):2136–47.
61. Harper LT, Turner TA, Warrior NA, Rudd CD. Characterisation of random carbon fibre composites from a directed fibre preforming process: the effect of fibre length. *Composites, Part A*. 2006;37(11):1863–78.
62. Warrior NA, Harper LT, Turner TA, Schubel PJ, Rudd CD, Kendall KN. Affordable lightweight body structures (ALBOS). In: JSAE Annual Congress; 2004; Pacifico, Yokohama.
63. Evans AD, Qian CC, Turner TA, Harper LT, Warrior NA. Flow characteristics of carbon fibre moulding compounds. *Composites, Part A*. 2016;90:1–12.
64. Kikuchi T, Fudauchi A, Koshino T, Narita C, Endo A, Takai Y, et al. Mechanical property of CFRP by carbon spray up method. In: Proceedings of the ASME 2013 International Mechanical Engineering Congress and Exposition; November 15–21, 2013. San Diego, California, USA.
65. Meyer O. Kurzfaser-Preform-Technologie zur kraftflussgerechten Herstellung von Faserverbundbauteilen (Short fiber preform technology for the load paths oriented production of fiber composite components). Stuttgart, Germany: University of Stuttgart; 2008.
66. Zin MH, Abdan K, Mazlan N, Zainudin ES, Liew KE, Norizan MN. Automated spray up process for pineapple leaf fibre hybrid biocomposites. *Compos Part B: Eng*. 2019;177:107306.
67. Hanafee ZM, Khalina A, Norkhairunnisa M, Edi Syams Z, Kan Ern L. The effect of different linear robot travel speed on mass flowrate of pineapple leaf fibre (PALF) automated spray up composite. *Compos Part B: Eng*. 2019;156:220–8.
68. Zin MH, Razzi MF, Othman S, Liew K, Abdan K, Mazlan N. A review on the fabrication method of bio-sourced hybrid composites for aerospace and automotive applications. *IOP Conf Series: Mater Sci Eng*. 2016;152:12041.
69. Hufenbach W, Gude M, Geller S, Czulak A. Manufacture of natural fiber-reinforced polyurethane composites using the long fiber injection process. *Polimery*. 2013;58(6):473–5.
70. Aßhoff C. Herstellung von »tailored composites« (production of »tailored composites«). Braunschweig, Germany: Fraunhofer-Institut für Holzforschung, Wilhelm-Kauditz-Institut WKI. [https://www.wki.fraunhofer.de/content/dam/wki/de/documents/Mediathek/infomaterial/flyer-und-themenblaetter/hofzet/WKI-Info\\_Tailored-Composites\\_2020-01\\_de.pdf](https://www.wki.fraunhofer.de/content/dam/wki/de/documents/Mediathek/infomaterial/flyer-und-themenblaetter/hofzet/WKI-Info_Tailored-Composites_2020-01_de.pdf) Accessed 10 April 2022
71. Hussain S, Kortschot M. A novel method to deliver natural fibre for mechanical reinforcement of polyurethane foam. *Cell Polym*. 2014;33(3):123–38.

72. Kikuchi T, Tani Y, Takai Y, Goto A, Hamada H. Biomechanics investigation of skillful technician in spray-up fabrication method: converting tacit knowledge to explicit knowledge in the fiber reinforced plastics molding. Digital human modeling. Applications in health, safety, ergonomics and risk management. Cham: Springer International Publishing; 2014. p. 24–34.
73. Kikuchi T, Tani Y, Takai Y, Goto A, Hamada H. Mechanical properties of jute composite by spray up fabrication method. Energy Procedia. 2014;56:289–97.
74. SCHMIDT & HEINZMANN GmbH & Co. KG. Be always one step ahead: Fiber spraying – breakthrough for bio-hybrid fiber composite materials. [https://schmidt-heinzmann.de/wp-content/uploads/2018/12/Case-Study-Fibre-Spraying\\_EN-02.2018.pdf](https://schmidt-heinzmann.de/wp-content/uploads/2018/12/Case-Study-Fibre-Spraying_EN-02.2018.pdf). Accessed 10 April 2022.
75. Lopes E, Fonseca de Campos P. Robotic digital fabrication of lightweight laminar prefabricated structures: the dragados case study in 1990's. In: 12th International Symposium on Ferrocement and Thin Cement Composites: The Technology on a Human Scale—FERRO12; January 2019. Belo Horizonte, Brazil.
76. Penin LF, Balaguer C, Pastor JM, Rodriguez FJ, Barrientos A, Aracil R. Robotized spraying of prefabricated panels. IEEE Robot Automat Mag. 1998;5(3):18–29.
77. Kozuka M. Sprühvorrichtung zur herstellung eines mit glasfasern verstärkten zementerzeugnisses (Spraying device for the production of a glass fiber reinforced product). Tokyo, Japan, German patent DE000002751661A1; 1977.
78. Schmidt E, Winkelbauer J, Puchas G, Henrich D, Krenkel W. Robot-based fiber spray process for small batch production. Annals of scientific society for assembly, handling and industrial robotics. Berlin, Heidelberg: Springer Berlin Heidelberg; 2020. p. 295–305.
79. Knohl S, Krenkel W, Puchas G, Wamser T. Ceramic composite materials and method for producing same. Munich, Germany. European patent EP 3 475 245 B1 (US patent 11,001,531 B2); 2017.
80. Schafföner S, Freitag L, Hubáľková J, Aneziris CG. Functional composites based on refractories produced by pressure slip casting. J Eur Ceram Soc. 2016;36(8):2109–17.
81. Montgomery DC. The 2<sup>k</sup> factorial design. Design and analysis of experiments. 8th ed. Hoboken, NJ: Wiley; 2013. p. 233–03
82. Kleppmann W. Vollständige faktorielle Versuchspläne (Full factorial design of experiments). Versuchsplanung: Produkte und Prozesse optimieren (Design of experiments: optimizing products and processes). 8th ed. München: Hanser; 2013. p. 101–27
83. 3M Advanced Materials Division. 3M™ Nextel™ ceramic fibers and textiles: technical reference guide. St. Paul, MN: 3M Advanced Materials Division; 2018.
84. DIN EN 658-3:2002-11, Hochleistungskeramik - Mechanische Eigenschaften von keramischen Verbundwerkstoffen bei Raumtemperatur - Teil\_3: Bestimmung der Biegefestigkeit; Deutsche Fassung EN\_658-3:2002: (advanced technical ceramics - mechanical properties of ceramic composites at room temperature - part 3: determination of flexural strength; German version EN 658-3:2002). Berlin: Beuth Verlag GmbH; 2002.
85. Levi CG, Zok FW, Yang J-Y, Mattoni M, Löfvander JPA. Microstructural design of stable porous matrices for all-oxide ceramic composites. Z Metallkd. 1999;90:1037–47.

**How to cite this article:** Winkelbauer J, Puchas G, Krenkel W, Schafföner S. Short fiber spraying process of all-oxide ceramic matrix composites: A parameter study. *Int J Appl Ceram Technol*. 2023;20:754–767. <https://doi.org/10.1111/ijac.14196>